

From 2D Images to 3D Model: Weakly Supervised Multi-View Face Reconstruction with Deep Fusion

Weiguang Zhao, Chaolong Yang, Jianan Ye, Yuyao Yan, Xi Yang and Kaizhu Huang

Abstract—We consider the problem of Multi-view 3D Face Reconstruction (MVR) with weakly supervised learning that leverages a limited number of 2D face images (e.g. 3) to generate a high-quality 3D face model with very light annotation. Despite their encouraging performance, present MVR methods simply concatenate multi-view image features and pay less attention to critical areas (e.g. eye, brow, nose, and mouth). To this end, we propose a novel model called Deep Fusion MVR (DF-MVR) and design a multi-view encoding to single decoding framework with skip connections, able to extract, integrate, and compensate deep features with attention from multi-view images. In addition, we develop a multi-view face parse network to learn, identify, and emphasize the critical common face area. Finally, though our model is trained with a few 2D images, it can reconstruct an accurate 3D model even if one single 2D image is input. We conduct extensive experiments to evaluate various multi-view 3D face reconstruction methods. Experiments on Pixel-Face and Bosphorus datasets indicate the superiority of our model. Without 3D landmarks annotation, DF-MVR achieves 5.2% and 3.0% RMSE improvement over the existing best weakly supervised MVRs respectively on Pixel-Face and Bosphorus dataset; with 3D landmarks annotation, DF-MVR attains superior performance particularly on Pixel-Face dataset, leading to 13.4% RMSE improvement over the best weakly supervised MVR model.

Index Terms—Face reconstruction, multi-view, face mask, 3DMM, Tri-Unet.

I. INTRODUCTION

RECONSTRUCTING 3D shapes of human faces from 2D images is a challenging yet essential task for numerous applications such as virtual reality, augmented reality, and facial animations [1, 2, 3]. 3D Morphable Model (3DMM) [4] is the pioneer in converting the 3D face model to a parameter representation. Recently, adopting convolutional neural networks (CNN) to extract 2D image information to predict 3DMM coefficients has become the mainstream method of face reconstruction. Supervised CNN-based methods [5, 6, 7] need a large number of 3D face meshes or point clouds corresponding to 2D pictures as groundtruth, which are time and/or manpower consuming.

To alleviate the need for 3D face meshes or point clouds data, recent efforts have shifted to weakly supervised and self-supervised methods [8, 9, 10, 11]. Most of these methods use landmarks and differentiable rendering for training. [8]

exploits the difference between each pixel of the original image and the rendered image as the loss. [10] attempts to combine pixelwise photometric difference and the skin probability mask to calculate the training loss.

All the above weakly supervised methods only exploit one single image for construction, which usually fails to estimate facial depth appropriately. For instance, the single-view reconstruction method [9, 12, 13] cannot fully explain the geometric difference of facial features, such as the height of the mouth and eye sockets. Such limitation can however be resolved by the geometric constraints contained in a few face images of different views, or multi-view images. Surprisingly, rare studies have been made on weakly supervised multi-view 3D face reconstruction tasks. To our best knowledge, Deep3DFace [10] and MGCNet [11] are the only methods currently available that utilize multi-view information from a single subject for weakly supervised reconstruction. Specifically, [10] scores each multi-view image using CNN and then selects the highest scoring image to regress shape parameters; [11] designs the consistency map based on multi-view consistency and calculates pixelwise photometric difference for the consistency map. Unfortunately, these two methods are limited because they simply concatenate multi-view image features and do not consider deep fusion of multi-view images features, nor do they pay attention to critical areas (e.g. eye, brow, nose, and mouth) which may impact the reconstruction quality the most.

To cope with these drawbacks, we propose a novel end-to-end weakly supervised multi-view 3D face reconstruction network which learns to fuse deep representations and identify critical areas. First, as multi-view images all represent the same face, we develop an encoding-decoding network (Tri-Unet) with attention to extract features and deeply fuse them into one feature map. As shown in Fig. 3, multiple encoders are used to extract features from multi-view images, and one single decoder is engaged to fuse these features in deep. In order to compensate for the possible loss caused by sampling, skip connections with attention are introduced. Second, we develop a multi-view face parse network to learn, identify, and emphasize the critical common face area. The novel face parse network is able to learn the face mask which not only acts as input features to help Tri-Unet encode/decode common area of multi-view images for better deep fusion, but also plays the role of a weight map to calculate the pixelwise photometric loss between rendered images and original images. Finally, we import RedNet [14] instead of ResNet [15], which is typically utilized in face reconstruction networks. RedNet is a residual network based on involution [14], which extracts more flexi-

W. Zhao, C. Yang, J. Ye are with Liverpool University, Liverpool L693BX, UK (e-mail: {W.Zhao30, C.Yang35, J.Ye16}@liverpool.ac.uk; Equal contribution: W. Zhao, C. Yang, J. Ye).

Y. Yan, X. Yang are with Xi'an Jiaotong-Liverpool University, Suzhou 215123, China (e-mail: xi.yang01@xjtlu.edu.cn, joshuayyy@gmail.com).

K. Huang is with Duke Kunshan University, Suzhou 215301, China (e-mail: kaizhu.huang@dukekunshan.edu.cn; Corresponding authors: K. Huang).

bly channel features than traditional convolution. Combining pixelwise photometric loss, mask loss, and landmark loss, we design a novel weakly supervised training framework that is able to fuse deep features comprehensively and pay attention to critical face features specially.

The contributions of our work are as follows:

- We design a novel weakly supervised encoding-decoding framework (Tri-Unet) for deep fusion of multi-view features, which has rarely been studied in the literature.
- We develop a face mask mechanism to identify common areas in multi-view images and encourage the 3D face reconstruction network to pay more attention to critical areas (e.g. eye, brow, nose, and mouth).
- Compared with traditional convolution, involution [14] is spatial-specific and able to obtain features on the channel, which means it can better process deep fusion features. We are the first to apply it to face reconstruction tasks.
- On the empirical side, our novel framework achieves 5.2% and 3.0% RMSE improvement over the existing best weakly supervised MVRs respectively on Pixel-Face and Bosphorus dataset without 3D landmarks annotation. In case of 3D landmarks annotation, DF-MVR attains superior performance, leading to 13.4% RMSE improvement on Pixel-Face dataset.

II. RELATED WORK

A. 3D Morphable Model

3D Morphable Model (3DMM) is a statistical model of 3D facial shape and texture which performs principal component analysis (PCA) on the face mesh training set [4]. Subsequently, [16] releases a generative 3D shape and texture model, the Basel Face Model (BFM), and demonstrates its application to several face recognition tasks. [17] has further expanded 3DMM to build models for specific ages, genders or ethnic groups. The current multi-view reconstruction methods mostly use BFM. For a fair comparison, we also exploit BFM to represent 3D faces in our model.

B. Single-view Methods

Most single-view face reconstruction methods take CNN as the deep learning network to predict 3DMM coefficients [18, 19]. For example, [20] deploys CNN to predict 3DMM coefficients and achieved encouraging results. [21] designs a robust method, based on CNN and ResNet101 [15], to regress 3DMM shape and texture coefficients directly from an input photo without annotation of landmarks. [22] concatenates the last two pooling layers of CNN to create a Fusion CNN branch for predicting the expression base individually. It also generates synthetic rendered face images with predicted 3D scans. However, these methods all require 3D mesh files as ground-truth, which greatly hinders their practical applications due to the shortfall of available annotated training data containing 3D shapes.

To cope with this issue, recent research focus has been put on weakly supervised and self-supervised methods. [8, 23] proposes a model that can be trained without 3D labels

by adopting differentiable rendering for calculating the pixel difference between the rendered image and the original image. [24] designs an end-to-end learning framework for accurately decomposing an unconstrained human face image into shape, reflectance and illuminance. [25] uses a similar method to predict 3D shapes while further adding GAN to generate more detailed texture information. [26] proposes to adopt the RGB-D image for face reconstruction, since depth information can enhance geometric constraints.

C. Multi-view Methods

Multi-view methods can provide more geometric constraints and structural information than single-view methods. [5] proposes to use Recurrent Neural Network (RNN) to fuse identity-related features extracted from deep convolutional neural network (DCNN) to produce more discriminative reconstructions, but their approach does not exploit multi-view geometric constraints. [27] adds multi-view geometric constraints and introduces the optical flow loss to improve the reconstruction accuracy. In the feature extraction of multiple images, they only concatenates the deep features. All these methods require ground-truth of 3DMM [5, 27], which is hardly available practically.

Surprisingly, there are few multi-view 3D face reconstruction methods based on weakly supervised machine learning in the literature. [10] designs two CNN models for predicting 3DMM coefficients and scoring each image. The image with high confidence is used to regress shape coefficients, and the rest images will be used to regress coefficients such as expression and texture. [11] adopts the concept of geometry consistency to design pixel and depth consistency loss. They establish dense pixel correspondences across multi-view input images and introduce the covisible maps to account for the self-occlusion. This method strengthens the attention to the common area of multiple images, but pays less attention to the local features of the face and the global features of multiple images. Our method employs the face parsing network to label the facial features of the face from multiple perspectives, which can not only focus on the common area of multiple perspectives, but also divide the common area in more detail.

III. MAIN METHODOLOGY

A. Overview

We first provide an overview of our proposed framework, which is shown in Fig. 1. We decide to exploit three multi-view images of a subject for generating a corresponding 3D face and introduce the *face parse network* (a) to process these three images separately to generate unified standard face masks. An *encoding-decoding network* (b) is designed to fuse the features of multi-view images in deep by sharing a decoder with an attention mechanism to obtain information from the encoder. Moreover, RedNet [14] is used as *parametric regression* (c) to regress 3DMM and pose coefficients. The reconstructed 3D face is reoriented utilizing the pose coefficients and then rendered back to 2D. The photo loss between the re-rendered 2D image and the input image at the target view is calculated while the masks are exploited as the weight map to enhance

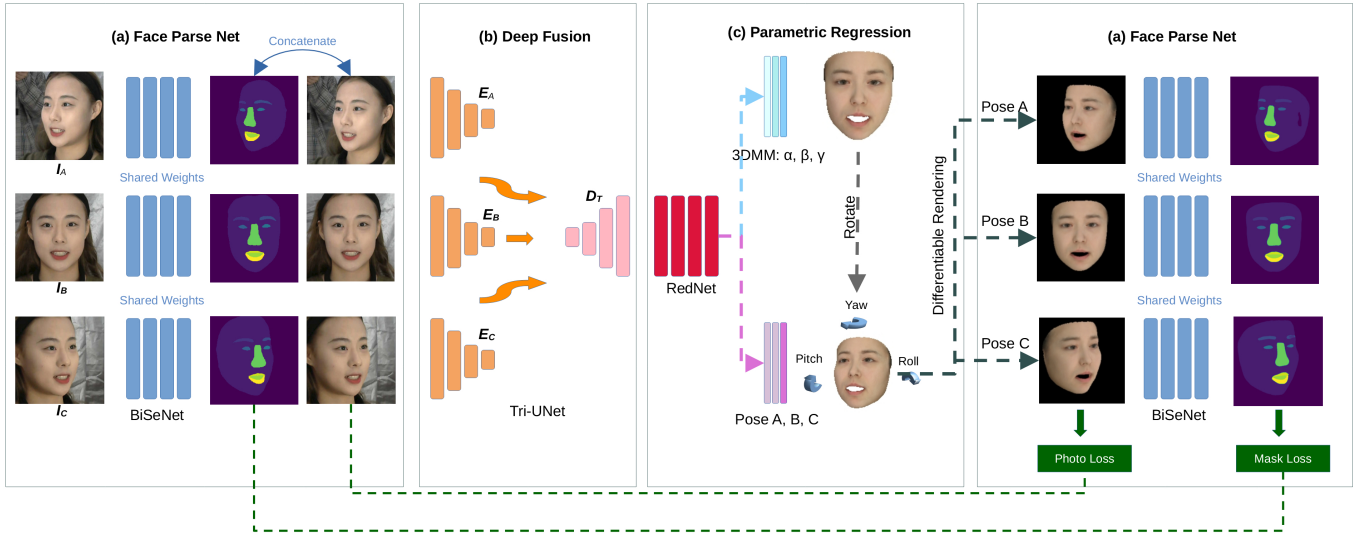


Fig. 1. Overview of DF-MVR

the back propagation of the facial features. In this section, we will provide details on each component as below.

B. Face Parse Net

We introduce the face parse network based on BiSeNet [28] to perform preliminary analysis of the input image and identify the elements of the image. The generated face mask has only one layer of channel. For example, if the size of the input image is $224 \times 224 \times 3$, the size of the face mask will be $224 \times 224 \times 1$. In order to better highlight the face, excessive elements of face masks such as hair and neck, will be removed, and the following parts will be kept: background, face skin, left brow, right brow, left eye, right eye, nose, mouth, upper lip, and lower lip. The reserved parts are marked with different numbers in order to distinguish facial features. As shown in Fig. 2, one-hot encoding is leveraged to assign the label for these parts. On one hand, the face masks are concatenated with the original images to help the network understand the common area of the multi-view image. On the other hand, the face masks serve as weight map to calculate the photo loss and mask loss for training.

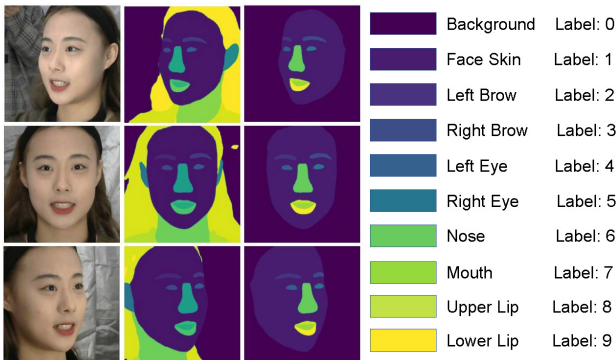


Fig. 2. Face Mask Annotation. In column order: original images, preliminary segmentation, face mask, legend.

C. Deep Fusion

The existing multi-view face reconstruction networks all deploy CNN or VGG [29] as the feature extractor. These networks concatenate the multi-graph features in the fully connected layer, which cannot perform feature interaction well. In addition, the previous networks mostly adopt shared weights or one backbone to process multi-view images, making it difficult for the network to pay attention to the unique information of each view. Differently, we design a novel feature fusion network, Tri-UNet, to extract features of multi-view images inspired by attention Unet [30].

We denote the three-view input images as I_A , I_B , and I_C , representing the three perspectives of left, front and right. Since the information and focus of each view are different, we set up three encoders to extract the features from three views respectively. Corresponding to the input images, these three encoders are represented by E_A , E_B , and E_C . The weights of the three encoders are not shared. Encoders are mainly composed of double convolution and maximum pooling. At the end of encoders, the deep features of I_A , I_B , I_C will be concatenated as F_D . Considering that I_A , I_B , and I_C actually describe the same object, we only set up a shared decoder for better fusing features as well as emphasizing the common features. The decoder is mainly composed of ConvTranspose, convolution, concatenate and skip connection. We adopt the attention mechanism to extract the feature F_A , F_B , and F_C from E_A , E_B , and E_C to enrich the information in the F_D decoding process. Finally, the fusion feature size we retain is $224 \times 224 \times 64$, in the case where the image size is $224 \times 224 \times 3$.

D. Parametric Regression

We adopt RedNet50 to process the fusion features and regress parameters. RedNet replaces traditional convolution with involution on the ResNet architecture. The inter-channel redundancy within the convolution filter stands out in many deep neural networks, casting the flexibility of convolution

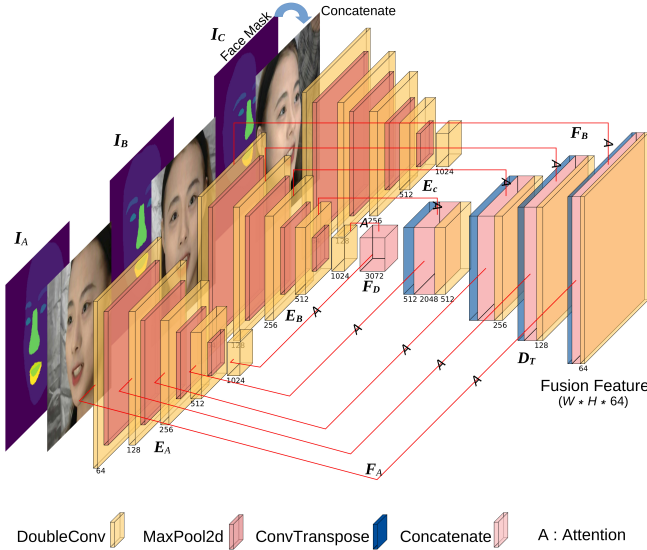


Fig. 3. Tri-UNet. For conciseness, we do not draw the skip connection of the E_C , which is similar to the E_A .

kernels w.r.t. different channels into doubt. Compared with traditional convolution, involution is spatial-specific and able to obtain features on the channel. Therefore, we choose Red-Net to perform parameter regression, and ablation experiments also verify its effectiveness.

3DMM Parameters regressed in this work include identification, expression, and texture parameters. The 3D face shape \mathbf{S} and the texture \mathbf{T} can be represented as:

$$\begin{aligned} \mathbf{S} &= \mathbf{S}(\alpha, \beta) = \bar{\mathbf{S}} + \mathbf{B}_{id}\alpha + \mathbf{B}_{exp}\beta, \\ \mathbf{T} &= \mathbf{T}(\gamma) = \bar{\mathbf{T}} + \mathbf{B}_t\gamma, \end{aligned} \quad (1)$$

where $\bar{\mathbf{S}}$ and $\bar{\mathbf{T}}$ are the average face shape and texture. \mathbf{B}_{id} , \mathbf{B}_{exp} , \mathbf{B}_t are the PCA bases of identity, expression, and texture respectively. α , β , and γ are the parameter vectors that the network needs to regress ($\alpha, \beta \in R^{80}$ and $\gamma \in R^{64}$). By adjusting these three vectors, the shape, expression and texture of the 3D face can be changed. In order to compare with MGCNet [11] and Deep3DFac [10] fairly, we use the same face model. BFM [16] is adopted for $\bar{\mathbf{S}}$, \mathbf{B}_{id} , $\bar{\mathbf{T}}$, and \mathbf{B}_t . \mathbf{B}_{exp} is built by [7] based on Facewarehouse [31].

Pose Parameters are used to adjust the angle and position of the 3D face in the camera coordinate system. We exploit the differentiable perspective rendering [32] to render the 3D face back to 2D. When the camera coordinates are fixed, we could change the size and angle of the rendered 2D face by adjusting the position of the 3D face in the camera coordinate system. Meanwhile, the position of the 3D face in the camera coordinate system can be determined by predicting the rotation angle and translation in each axis. In order to enhance the geometric constraints of the multi-view reconstruction, we respectively predict the pose of the 3D faces in the multi-view, instead of only predicting the pose of one perspective to render 2D images.

In this framework, two training schemes are proposed: weakly supervised and self-monitored training, depending on whether or not 3D landmarks are utilized. As a weakly

supervised training method, our model needs to work with slight 3D annotations as labels. On the other hand, if 3D landmarks are not introduced to calculate the loss, our model will not require any 3D labels and only require multi-view images for training. Both the schemes have been verified and compared in the following sections.

IV. WEAKLY SUPERVISED TRAINING

In order to alleviate the strong need for the labeled data, we design a weakly supervised method for training. First, we render the predicted 3D face model back to 2D and compare the rendered image with the original image pixel by pixel. Then, the rendered 2D images are fed into the face parse network to generate rendered face masks. According to the consistency principle, the rendered face masks should be consistent with the original face masks. Therefore, the L2 distance is treated as a mask loss. Finally, the landmark loss and regularization loss are introduced to shape 3D face and suppress the generation of distorted faces.

A. Photo Loss

Photo loss is often used in weakly supervised face reconstruction tasks [10, 11, 13, 33]. Distinct with the traditional methods, we impose a weight for each pixel according to the facial features. The weight map is learned by the face mask \mathcal{M} of the original image I . In order to enhance the robustness of the weight map, we dilate \mathcal{M} with 20 pixel as \mathcal{M}_d , as shown in Fig. 4. The dilated image is divided into three levels to be the weight map. In weight map, facial features are marked as 254, the rest of the facial area is marked as 128, and the background is marked as 32. The multi-view photo loss can be expressed as:

$$L_p = \frac{1}{\mathcal{V}} \sum_{v=1}^{\mathcal{V}} \frac{\sum_{i \in \mathcal{P}^v} \mathcal{M}_{di}^v \cdot \|I_i^v - I_i^{v'}\|_2}{\sum_{i \in \mathcal{P}^v} \mathcal{M}_{di}^v}, \quad (2)$$

where \mathcal{V} is the number of the reconstructed views. \mathcal{V} is 3 in the proposed model. \mathcal{P}^v is the area where the rendered image $I^{v'}$ and the original image I^v intersect in the current view. i denotes pixel index, and $\|\cdot\|_2$ denotes the L2 norm.

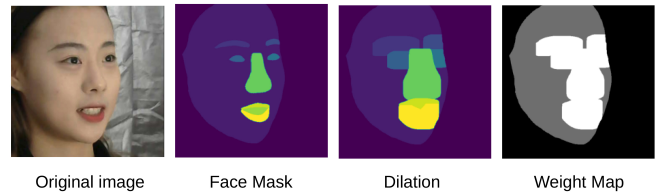


Fig. 4. Weight Map

B. Mask Loss

Photo loss focuses on the pixel difference between two pictures. It is difficult to constrain the size of the facial feature area in the two pictures. For example, the nose color is very similar to that of the cheeks, thereby leading to difficulties for the photo loss to notice the boundary line between them.

For this reason, we introduce mask loss to narrow the facial features of the input image and the rendered image. The division and labeling of the facial features are shown in Fig. 2. According to [28] we adopt cross entropy to calculate the mask loss L_m :

$$L_m = -\frac{1}{N_p V} \sum_{v=1}^V \sum_{p=1}^{N_p} (y_p \log(\hat{y}_p) + (1 - y_p) \log(1 - \hat{y}_p)), \quad (3)$$

where N_p is number of pixels in face mask. \hat{y}_p donates the category prediction of pixels in face mask and y_p is the label.

C. Landmark Loss

We also adopt 2D landmarks and 3D landmarks for weakly supervised training. We use 3D face alignment method [34] to generate 68 landmarks $\{l_n\}$ as the groundtruth. Then the corresponding points in the predicted 3D face point cloud are projected to 2D as predicted 2D landmarks $\{l'_n\}$. Then the multi-view 2D landmark loss can be calculated:

$$L_{l_{2d}} = \frac{1}{NV} \sum_{v=1}^V \sum_{n=1}^N \omega_n \|l_n^v - l'_n\|_2, \quad (4)$$

where ω_n is the weight for each landmark. We set the weight to 20 only for the nose and inner mouth landmarks, and to 1 otherwise.

2D landmarks are still insufficient for the reconstruction of 3D face shapes. In order to obtain better reconstruction effect, we select 101 3D landmarks $\{q'_n\}$ to impose a weak constraint on the shape of the 3D face. According to the 3DMM index, 101 predicted landmarks $\{q_n\}$ can be found. Then, we select 7 points $\{a'_n\}$ and $\{a_n\}$ in $\{q'_n\}$ and $\{q_n\}$ respectively as alignment points to calculate the alignment parameters of $\{q'_n\}$ and $\{q_n\}$. The alignment parameters include: scale s , rotation \mathbf{R} and translation \mathbf{t} . These parameters can be obtained by the following optimization equation [35, 36]:

$$Optim(s, \mathbf{R}, \mathbf{t}) = \min_{s, \mathbf{R}, \mathbf{t}} \sum_i \|a'_i - s(\mathbf{R} \cdot \mathbf{a}_i + \mathbf{t})\|_2. \quad (5)$$

After the optimal s , \mathbf{R} and \mathbf{t} are obtained, the predicted 101 landmarks $\{q_n\}$ can be converted to the space of $\{q'_n\}$ as $\{q_{nt}\} = s(\mathbf{R} \cdot \mathbf{q}_n + \mathbf{t})$.

Then the multi-view 3D landmark loss can be calculated:

$$L_{l_{3d}} = \frac{1}{N} \sum_{n=1}^N \|q_{nt} - q'_n\|_2. \quad (6)$$

In summary, the landmark loss can be expressed as:

$$L_l = \omega_{2d} L_{l_{2d}} + \omega_{3d} L_{l_{3d}}, \quad (7)$$

where ω_{2d} and ω_{3d} represent respectively the weight of 2D landmark loss and 3D landmark loss. In this work, we set them to 0.02 and 1 as tuned empirically.

D. Regularization Loss

To suppress the generation of distorted faces, we add the regularization loss which is commonly-used in face reconstruction task [10, 11, 13, 33]:

$$L_{reg} = \omega_\alpha \|\alpha\|^2 + \omega_\beta \|\beta\|^2 + \omega_\gamma \|\gamma\|^2, \quad (8)$$

where α , β , and γ are 3DMM parameter vectors that the network predicted. ω_α , ω_β and ω_γ are the weights for 3DMM parameter vectors. Following Deep3DFace [10], we set them to 1, 0.8 and 0.017 with fine tuning.

E. Overall Loss

The overall loss required by our end-to-end net for weakly supervised training can be represented as:

$$L_{all} = \omega_p L_p + \omega_m L_m + \omega_l L_l + \omega_{reg} L_{reg},$$

where ω_p , ω_m , ω_l , ω_{reg} are the weights for photo loss, mask loss, landmark loss and regularization loss. Following Deep3DFace, we set $\omega_{reg} = 3.0 \times 10^{-4}$. Since ω_{2d} and ω_{3d} have been determined, we just fix $\omega_l = 1$ to adjust ω_p and ω_m by sensitivity analysis. Then, we set $\omega_p = 4$ and $\omega_m = 3$ as empirically obtained in sensitivity analysis.

V. EXPERIMENT

A. Setup

Dataset. Following BiseNet [28], we adopt CelebAMask-HQ [37] to pretrain Face Parse Net. Furthermore, Pixel-Face [38] and Multi-PIE [39] are introduced to provide 3D landmarks label and multi-view faces. Pixel-Face contains 855 subjects ranging in age from 18 to 80 years old. Each subject has 7 or 23 samples of different expressions. Pixel-Face has 3D mesh file of each sample as groundtruth but not 3DMM parameters or angle of multi-view images. Hence, it is suitable for weakly supervised or unsupervised training for MVR. In the experiment, the training/test split was set to 0.8. For Multi-PIE, we leverage the version provided by [40], which will reduce a lot of data preprocessing work. This dataset contains about 140k multi-view images and does not provide 3D mesh and landmarks. We utilize the method of [41] to detect and align faces. Then each input image is cropped and resized to 224×224 .

Network. Our network structure is shown in Fig. 1 and described in the methodology section. Based on the pre-trained BiseNet [28] with frozen weights, the face parse network is located in the beginning and end of the network. In the scenario of MVR, we design a fusion network consisting of three different encoders to emphasize more diverse features. A lightweight RedNet50 [14] is designed as the parameter regression network, since the fusion network has already extracted sufficient information. We implement DF-MVR by pytorch [42]. It is trained on 2 NVIDIA RTX 3090 GPUs card with a batch size of 16 for 512 epochs. We adopt Adam [43] as the gradient descent method. The initial learning rate is set to 0.0001 which decays with the cosine anneal schedule [44]. The average inference time of DF-MVR is 244ms.

Evaluation Metric. Following the previous works, RMSE (mm) [10, 11, 27] is used to compute point-to-plane L2 distance between predict 3D scans and groundtruth 3D scans. Concretely, the front face area is cropped for metrics calculation instead of using a complete BFM model [10, 11, 36]. Before calculating point-to-plane L2 distance, the predicted 3D scans need to be registered with ground-truth 3D scans. Also, we take the ICP registration method [45], the same as [10].

B. Comparison to SOTAs

We compare our method with the existing weakly supervised MVRs both on Pixel-Face and Bosphorus datasets. More specifically, only the two methods can be found in the literature related to multi-view weakly supervised 3D face reconstruction, both of which are used as the comparison methods in this paper. [11] uses multiple images for training, and then a single image for testing. We select the best results among the three images for display. [10] does not release their source codes of its scoring network. We use their codes to train/test on Pixel-Face.

Comparison on Pixel-Face. The quantitative results of the comparison are shown in Table I. As observed, our proposed model attains the superior performance, leading to 13.4% RMSE improvement over the existing best weakly supervised MVRs. Since [11] and [10] did not use 3D landmarks, to be fair, we also provide the results of our model without using 3D landmarks for comparison. Our model (without 3D landmarks) shows 5.2% improvement compared to the existing methods with the even highest stability according to the standard deviation.

TABLE I
QUANTITATIVE COMPARISON ON PIXEL-FACE.

Method	Dataset	Mean	Std
Shang et al. [11]	Pixel-Face	1.8877	0.4378
Deng et al. [10]	Pixel-Face	1.6641	0.3690
Ours (w/o $L_{l,3d}$)	Pixel-Face	1.5770	0.2157
Ours	Pixel-Face	1.4402	0.2959

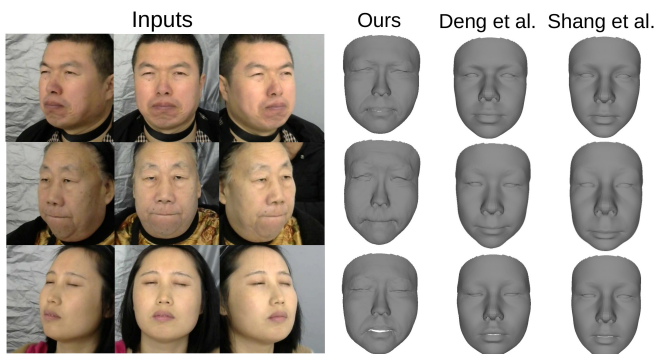


Fig. 5. Qualitative Comparison on Pixel-Face

The visual comparison is shown in Fig. 5 given 3-view faces. It is evident that our predicted model is more accurate, especially in terms of facial depth estimation in the facial

features. In addition, our model can better learn human facial expressions, such as closing eyes and pursing lips.

Comparison on Bosphorus. Since Pixel-Face dataset is collected based on Asian faces, the samples it contains are limited by regions. On the other hand, Pixel-Face dataset is only made under one lighting environment and three fixed camera angles. Taking into account the diversity, we adopt the richer Multi-PIE dataset for training and Bosphorus dataset for testing. Both datasets contain faces across continents and are collected in various lighting environments and shooting angles. Because Multi-PIE does not provide 3D landmarks, we remove $L_{l,3d}$ to train DF-MVR for this part. Delaunay algorithm [46] is utilized to generate mesh files from point clouds for Bosphorus dataset. We set the left and right inputs to 45 degrees for comparison. More angle robustness experiments can be later seen in Table V. The quantitative results of the comparison are shown in Table II. Our model (without 3D landmarks) exhibits 3.0% improvement compared to the existing methods. The qualitative comparison is also provided in Fig. 6.

TABLE II
QUANTITATIVE COMPARISON ON BOSPHORUS.

Method	Dataset	Mean	Std
Shang et al. [11]	Bosphorus	1.4418	0.3384
Deng et al. [10]	Bosphorus	1.4777	0.3432
Ours (w/o $L_{l,3d}$)	Bosphorus	1.3994	0.3930

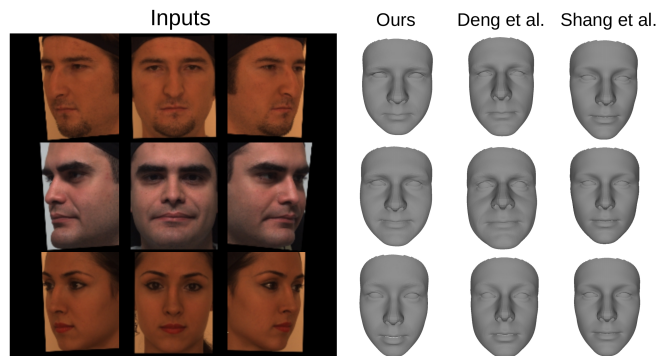


Fig. 6. Qualitative Comparison on Bosphorus

Visual Comparison without 3D landmarks. A closer qualitative comparison is shown in Fig. 7 in the case of no 3D landmarks. Because 3D landmarks will improve the reconstruction of facial features, for fairness, we also report the results (without 3D landmarks) for comparison, which can better reflect the effect of face mask mechanism on facial feature adjustment. In the first sample, our model can predict the expression of pursed lips. The upper lip of our model is almost invisible, compared to the other models. In the second sample, the eyebrows and eyes of our model appear more similar to those of the original image.

C. Single-view Reconstruction.

The single-view reconstruction method only requires one image to generate the 3D face. From the practical viewpoint, it is more flexible though it may be inferior to multi-view

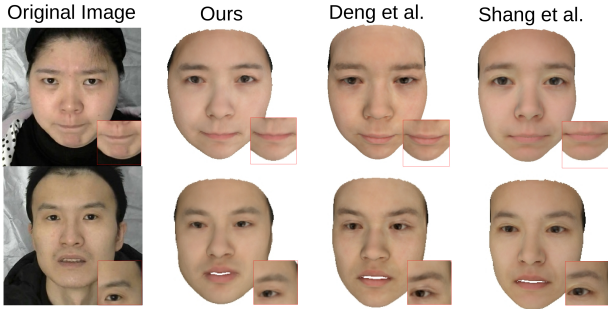


Fig. 7. Detailed Comparison

methods in terms of accuracy. Our method can also be adapted in the single view scenario. More specifically, during the training process, we only change the input, without changing other parts. As shown in Fig. 8, the original input has been changed to four different forms, according to the probability: P'_a, P_1, P_f, P_r . The input of multi-view images still needs to be dominant to preserve accuracy, so we set its probability to 2/3, and the other inputs equally distribute with the probability of 1/3.

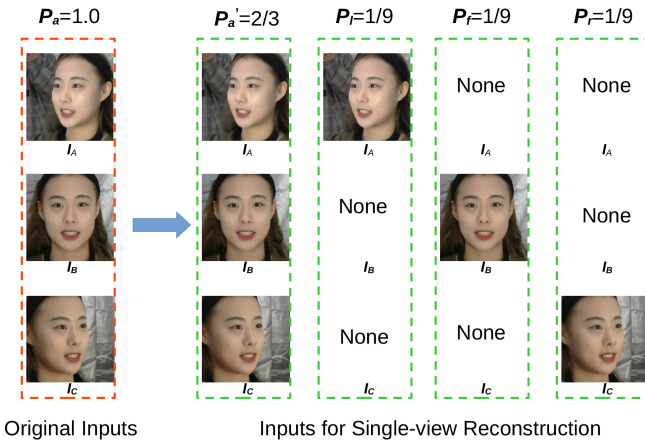


Fig. 8. Inputs for Single-view Reconstruction. 'None' means a black image.

The parameterized results of the comparison are shown in Table III. As observed, our proposed model also attains the superior performance. In the case of single image testing, our model is more effective than [10] and [11]. More specifically, [11] adopted multiple images for training, and then a single image for testing, which is the same as our model in the case of sing-view. [10] does not release their source codes of their scoring network. We use their codes to train/test on Pixel-Face. Visual comparisons are shown in Fig. 9.

TABLE III
COMPARISON OF RMSE (MM)

Method	Dataset	Mean	Std
Shang et al. [11]	Pixel-Face	1.8877	0.4378
Deng et al. [10]	Pixel-Face	1.6641	0.3690
Ours (single-view)	Pixel-Face	1.5437	0.3088
Ours	Pixel-Face	1.4738	0.3059

It can also be seen from Fig. 9 that our model is more sensitive to depth changes. The mouths and cheeks reconstructed by our model are more accurate. On the other hand, the three 3D faces reconstructed from multi-view in [11] have greater differences, while the three 3D faces reconstructed by our method from multi-view appear more similar.

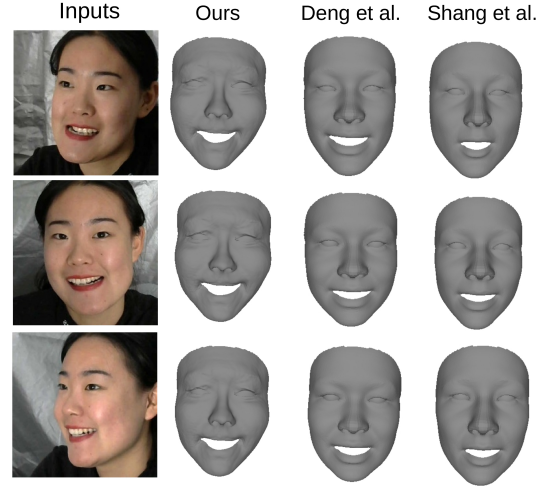


Fig. 9. Comparisons to SOTA Methods. We only input one image to the network.

D. Ablation Study

In order to verify the effectiveness of Tri-UNet and the mask mechanism we designed, we perform more ablation experiments as shown in Table IV. The mean and standard deviation of RMSE are again used as the evaluation metric. First, from v1, v2, v6, it can be found that the multi-view feature fusion network we designed is superior to traditional CNN and UNet in this task. Then, the results of v2 and v6 hint that the multi-layer feature interaction in the feature extraction stage is better than the direct concatenation of features at the end. To be fair, we set the number of layers of RedNet and ResNet to 50. Through the RMSE of v3 and v6, it is clear that RedNet performs better than ResNet in this task. For v4, we not only remove the mask loss but also the face mask I_A, I_B and I_C , which are concatenated to the original image. By comparing v5 and v6, we can see that the face mask mechanism promotes the network to generate a higher-precision model. Moreover, we verify the face mask and mask loss separately. Mask loss has a much smaller effect on the accuracy of the model than face mask. While the qualitative result of mask loss is positive for the adjustment of the model during training, we retain this part for reference. Finally, we remove L_{lan_3d} , which means that our model can be trained with only three multi-view images without any 3D label (as denoted as v5). The result also shows that our model is accurate and stable.

As shown in Fig. 10, we select 3 representative samples from the verification set for visualization [47]. The first sample is an elderly person with one eye open and one eye closed. From the results, our model can predict her skin color and

TABLE IV
ABLATION STUDY

Ours	Backbone	/	Facemask	L_{l_3d}	Mean	Std
v1	CNN	RedNet	Y	Y	1.5415	0.3120
v2	Unet	RedNet	Y	Y	1.5207	0.3063
v3	Tri-Unet	ResNet	Y	Y	1.5206	0.3174
v4	Tri-Unet	RedNet	N	Y	1.4656	0.3088
v5	Tri-Unet	RedNet	Y	N	1.5770	0.2157
v6	Tri-Unet	RedNet	Y	Y	1.4402	0.2959

expression with smaller error. Due to the limitations of the 3DMM shape vector base, her wrinkles cannot be refined. The other two samples are angry young women and calm middle-aged man. More qualitative results are provided in the appendix.

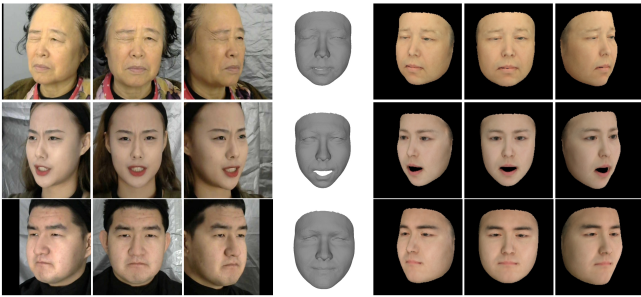


Fig. 10. DF-MVR Result (v6) with 3DMM Texture. The first three columns are the input images. The fourth column is the 3D face reconstructed by DF-MVR (w/o texture). The last three columns are the rendered images after reconstructing the face.

E. Sensitivity Analysis

We take Pixel-Face dataset for one typical example to analyze the parameter sensitivity and examine if the coefficients of the photo loss and mask loss have impact on the model performance. In order to ensure the accuracy of the model, we perform parameter sensitivity analysis on ω_p and ω_m . As shown in Fig. 11, we first fix the other parameters and only change ω_p . When ω_p is between 4 and 5, the model can obtain higher accuracy. Then, we fix ω_p at 4 and only change ω_m . When ω_m is near 3, the model can obtain higher accuracy. In this way, we set ω_p and ω_m to 4 and 3 respectively.

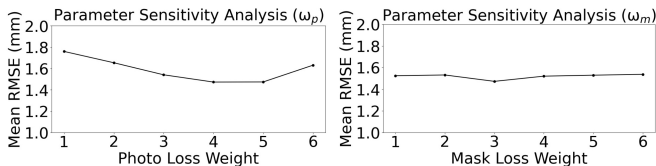


Fig. 11. Sensitivity Analysis

F. Robustness Analysis

Multi-PIE and Bosphorus are collected by different cameras. DF-MVR uses Multi-PIE for training and achieves good test results on Bosphorus, which implies that our model has a

certain robustness to camera device changes. Moreover, we further explore robustness of DF-MVR for shooting angles. We fix the I_B and I_C face angles while adjusting the I_A face angle. Table V and Fig. 12 show that our model consistently achieve the best results in different shooting angles, implying that our model exhibits the best robustness. Random means we choose the degree from 10° , 20° , 30° and 45° randomly. The light environment is also random in this experiment.

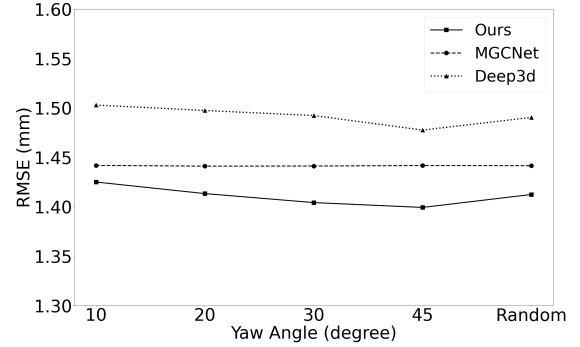


Fig. 12. Robustness Analysis

TABLE V
ROBUSTNESS ANALYSIS ON BOSPHORUS.

Method	10°	20°	30°	45°	Random
Shang et al. [11]	1.4419	1.4412	1.4413	1.4418	1.4416
Deng et al. [10]	1.5030	1.4975	1.4924	1.4777	1.4905
Ours (v5)	1.4251	1.4134	1.4043	1.3994	1.4125

We also validate the angle robustness of our model visually. These results are plotted in Fig. 13. Detailed error maps are introduced to display the error for each facial area directly. Take the second sample of Fig. 6 for a typical example where we fix I_B and I_C while changing the face angle of I_A from 10° to 45° . Obviously, the error maps generated from these angles do not change much. Furthermore, we provide the error maps of [10] for comparison. At different angles, DF-MVR reconstructs the face with less error, especially in critical areas (e.g. eye, brow, nose and mouth).

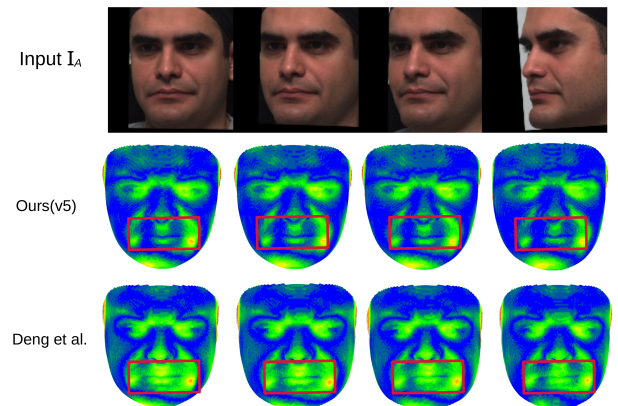


Fig. 13. Reconstruction Error Maps. The errors are expressed from small to large in the following order: blue, green, yellow, red.

G. Limitations and Future Work.

While achieving higher accuracy and enjoying view robustness, our model also has some limitations. Particularly, our model is based on 3DMM which has finite vector base (\mathbf{B}_{id} , \mathbf{B}_{exp} and \mathbf{B}_t). To this end, our model might not reconstruct wrinkles, beards, eye shadow, etc., as shown in Fig. 14. We will focus on solving this problem in the future.

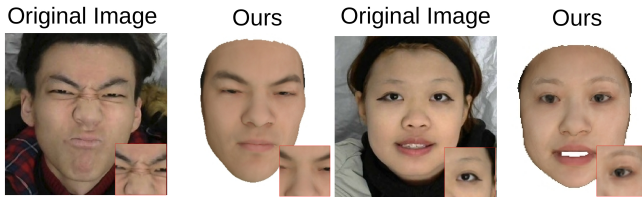


Fig. 14. Some Challenging Cases

VI. CONCLUSION

In this paper, we design a novel end-to-end weakly supervised multi-view 3D face reconstruction network that exploits multi-view encoding to a single decoding framework with skip connections, able to extract, integrate, and compensate deep features with attention. In addition, we develop a multi-view face parse network to learn, identify, and emphasize the critical common face area. Combining pixelwise photometric loss, mask loss, and landmark loss, we complete the weakly supervised training. Extensive experiments verify the effectiveness of our model.

REFERENCES

- [1] Robin Andlauer, Andreas Wachter, Matthias Schaufelberger, Frederic Weichel, Reinald Kühle, Christian Freudlsperger, and Werner Nahm. 3d-guided face manipulation of 2d images for the prediction of post-operative outcome after cranio-maxillofacial surgery. *IEEE Transactions on Image Processing (TIP)*, 30:7349–7363, 2021. doi: 10.1109/TIP.2021.3096081.
- [2] Feng Liu, Qijun Zhao, Xiaoming Liu, and Dan Zeng. Joint face alignment and 3d face reconstruction with application to face recognition. *IEEE Transactions on Pattern Analysis and Machine Intelligence (TPAMI)*, 42(3):664–678, 2020. doi: 10.1109/TPAMI.2018.2885995.
- [3] Zhihan Lv. Robust3d: a robust 3d face reconstruction application. *Neural Computing and Applications*, 32:8893–8900, 2019.
- [4] Volker Blanz and Thomas Vetter. A morphable model for the synthesis of 3d faces. In *Proceedings of the Annual Conference on Computer Graphics and Interactive Techniques (SIGGRAPH)*, pages 187–194, 1999.
- [5] Pengfei Dou and Ioannis A Kakadiaris. Multi-view 3d face reconstruction with deep recurrent neural networks. *Image and Vision Computing*, 80:80–91, 2018.
- [6] Yao Feng, Fan Wu, Xiaohu Shao, Yanfeng Wang, and Xi Zhou. Joint 3d face reconstruction and dense alignment with position map regression network. In *Proceedings of the European Conference on Computer Vision (ECCV)*, pages 534–551, 2018.
- [7] Yudong Guo, Jianfei Cai, Boyi Jiang, Jianmin Zheng, et al. Cnn-based real-time dense face reconstruction with inverse-rendered photo-realistic face images. *IEEE Transactions on Pattern Analysis and Machine Intelligence (TPAMI)*, 41(6):1294–1307, 2018.
- [8] Ayush Tewari, Michael Zollhofer, Hyeonwoo Kim, Pablo Garrido, Florian Bernard, Patrick Perez, and Christian Theobalt. Mofa: Model-based deep convolutional face autoencoder for unsupervised monocular reconstruction. In *Proceedings of the IEEE International Conference on Computer Vision Workshops (ICCVW)*, pages 1274–1283, 2017.
- [9] Anh Tuan Tran, Tal Hassner, Iacopo Masi, Eran Paz, Yuval Nirkin, and Gérard G Medioni. Extreme 3d face reconstruction: Seeing through occlusions. In *Proceedings of the IEEE Conference on Computer Vision and Pattern Recognition (CVPR)*, pages 3935–3944, 2018.
- [10] Yu Deng, Jiaolong Yang, Sicheng Xu, Dong Chen, Yunde Jia, and Xin Tong. Accurate 3d face reconstruction with weakly-supervised learning: From single image to image set. In *Proceedings of the IEEE Conference on Computer Vision and Pattern Recognition Workshops (CVPRW)*, pages 0–0, 2019.
- [11] Jiaxiang Shang, Tianwei Shen, Shiwei Li, Lei Zhou, Mingmin Zhen, Tian Fang, and Long Quan. Self-supervised monocular 3d face reconstruction by occlusion-aware multi-view geometry consistency. In *Proceedings of the European Conference on Computer Vision (ECCV)*, pages 53–70. Springer, 2020.
- [12] Elad Richardson, Matan Sela, Roy Or-El, and Ron Kimmel. Learning detailed face reconstruction from a single image. In *Proceedings of the IEEE Conference on Computer Vision and Pattern Recognition (CVPR)*, pages 1259–1268, 2017.
- [13] Ayush Tewari, Michael Zollhöfer, Pablo Garrido, Florian Bernard, Hyeonwoo Kim, Patrick Pérez, and Christian Theobalt. Self-supervised multi-level face model learning for monocular reconstruction at over 250 hz. In *Proceedings of the IEEE Conference on Computer Vision and Pattern Recognition (CVPR)*, pages 2549–2559, 2018.
- [14] Duo Li, Jie Hu, Changhu Wang, Xiangtai Li, Qi She, Lei Zhu, Tong Zhang, and Qifeng Chen. Involution: Inverting the inherence of convolution for visual recognition. In *Proceedings of the IEEE Conference on Computer Vision and Pattern Recognition (CVPR)*, pages 12321–12330, 2021.
- [15] Kaiming He, Xiangyu Zhang, Shaoqing Ren, and Jian Sun. Deep residual learning for image recognition. In *Proceedings of the IEEE Conference on Computer Vision and Pattern Recognition (CVPR)*, pages 770–778, 2016.
- [16] Pascal Paysan, Reinhard Knothe, Brian Amberg, Sami Romdhani, and Thomas Vetter. A 3d face model for pose and illumination invariant face recognition. In *Proceedings of the IEEE International Conference on Advanced Video and Signal Based Surveillance (AVSS)*, pages 296–301, 2009.
- [17] James Booth, Anastasios Roussos, Allan Ponniah, David Dunaway, and Stefanos Zafeiriou. Large scale 3d mor-

- phable models. *International Journal of Computer Vision (IJCV)*, 126(2):233–254, 2018.
- [18] Mingli Song, Dacheng Tao, Xiaoqin Huang, Chun Chen, and Jiajun Bu. Three-dimensional face reconstruction from a single image by a coupled rbf network. *IEEE Transactions on Image Processing (TIP)*, 21(5):2887–2897, 2012. doi: 10.1109/TIP.2012.2183882.
- [19] Yajing Chen, Fanzi Wu, Zeyu Wang, Yibing Song, Yonggen Ling, and Linchao Bao. Self-supervised learning of detailed 3d face reconstruction. *IEEE Transactions on Image Processing*, 29:8696–8705, 2020. doi: 10.1109/TIP.2020.3017347.
- [20] Xiangyu Zhu, Zhen Lei, Xiaoming Liu, Hailin Shi, and Stan Z Li. Face alignment across large poses: A 3d solution. In *Proceedings of the IEEE Conference on Computer Vision and Pattern Recognition (CVPR)*, pages 146–155, 2016.
- [21] Anh Tuan Tran, Tal Hassner, Iacopo Masi, and Gerard Medioni. Regressing robust and discriminative 3d morphable models with a very deep neural network. In *Proceedings of the IEEE Conference on Computer Vision and Pattern Recognition (CVPR)*, pages 5163–5172, 2017.
- [22] Pengfei Dou, Shishir K Shah, and Ioannis A Kakadiaris. End-to-end 3d face reconstruction with deep neural networks. In *Proceedings of the IEEE Conference on Computer Vision and Pattern Recognition (CVPR)*, pages 5908–5917, 2017.
- [23] Kyle Genova, Forrester Cole, Aaron Maschinot, Aaron Sarna, Daniel Vlasic, and William T Freeman. Unsupervised training for 3d morphable model regression. In *Proceedings of the IEEE Conference on Computer Vision and Pattern Recognition (CVPR)*, pages 8377–8386, 2018.
- [24] Soumyadip Sengupta, Angjoo Kanazawa, Carlos D Castillo, and David W Jacobs. Sfsnet: Learning shape, reflectance and illuminance of faces in the wild’. In *Proceedings of the IEEE Conference on Computer Vision and Pattern Recognition (CVPR)*, pages 6296–6305, 2018.
- [25] Jiangke Lin, Yi Yuan, Tianjia Shao, and Kun Zhou. Towards high-fidelity 3d face reconstruction from in-the-wild images using graph convolutional networks. In *Proceedings of the IEEE Conference on Computer Vision and Pattern Recognition (CVPR)*, pages 5891–5900, 2020.
- [26] Yudong Guo, Lin Cai, and Juyong Zhang. 3d face from x: Learning face shape from diverse sources. *IEEE Transactions on Image Processing (TIP)*, 30:3815–3827, 2021. doi: 10.1109/TIP.2021.3065798.
- [27] Fanzi Wu, Linchao Bao, Yajing Chen, Yonggen Ling, Yibing Song, Songnan Li, King Ngi Ngan, and Wei Liu. Mvf-net: Multi-view 3d face morphable model regression. In *Proceedings of the IEEE Conference on Computer Vision and Pattern Recognition (CVPR)*, pages 959–968, 2019.
- [28] Changqian Yu, Jingbo Wang, Chao Peng, Changxin Gao, Gang Yu, and Nong Sang. Bisenet: Bilateral segmentation network for real-time semantic segmentation. In *Proceedings of the European conference on computer vision (ECCV)*, pages 325–341, 2018.
- [29] Karen Simonyan and Andrew Zisserman. Very deep convolutional networks for large-scale image recognition. *ArXiv Preprint ArXiv:1409.1556*, 2014.
- [30] Ozan Oktay, Jo Schlemper, Loic Le Folgoc, Matthew Lee, Mattias Heinrich, Kazunari Misawa, Kensaku Mori, Steven McDonagh, Nils Y Hammerla, Bernhard Kainz, et al. Attention u-net: Learning where to look for the pancreas. *ArXiv Preprint ArXiv:1804.03999*, 2018.
- [31] Chen Cao, Yanlin Weng, Shun Zhou, Yiyong Tong, and Kun Zhou. Facewarehouse: A 3d facial expression database for visual computing. *IEEE Transactions on Visualization and Computer Graphics (T-VCG)*, 20(3): 413–425, 2013.
- [32] Nikhila Ravi, Jeremy Reizenstein, David Novotny, Taylor Gordon, Wan-Yen Lo, Justin Johnson, and Georgia Gkioxari. Accelerating 3d deep learning with pytorch3d. *ArXiv Preprint ArXiv:2007.08501*, 2020.
- [33] Justus Thies, Michael Zollhofer, Marc Stamminger, Christian Theobalt, and Matthias Nießner. Face2face: Real-time face capture and reenactment of rgb videos. In *Proceedings of the IEEE Conference on Computer Vision and Pattern Recognition (CVPR)*, pages 2387–2395, 2016.
- [34] Adrian Bulat and Georgios Tzimiropoulos. How far are we from solving the 2d & 3d face alignment problem? (and a dataset of 230,000 3d facial landmarks). In *Proceedings of the IEEE International Conference on Computer Vision (ICCV)*, 2017.
- [35] Gary KL Tam, Zhi-Quan Cheng, Yu-Kun Lai, Frank C Langbein, Yonghuai Liu, David Marshall, Ralph R Martin, Xian-Fang Sun, and Paul L Rosin. Registration of 3d point clouds and meshes: A survey from rigid to nonrigid. *IEEE Transactions on Visualization and Computer Graphics (T-VCG)*, 19(7):1199–1217, 2012.
- [36] Soubhik Sanyal, Timo Bolkart, Haiwen Feng, and Michael J Black. Learning to regress 3d face shape and expression from an image without 3d supervision. In *Proceedings of the IEEE Conference on Computer Vision and Pattern Recognition (CVPR)*, pages 7763–7772, 2019.
- [37] Cheng-Han Lee, Ziwei Liu, Lingyun Wu, and Ping Luo. Maskgan: Towards diverse and interactive facial image manipulation. In *Proceedings of the IEEE Conference on Computer Vision and Pattern Recognition (CVPR)*, 2020.
- [38] Jiangjing Lyu, Xiaobo Li, Xiangyu Zhu, and Cheng Cheng. Pixel-face: A large-scale, high-resolution benchmark for 3d face reconstruction. *ArXiv Preprint ArXiv:2008.12444*, 2020.
- [39] Ralph Gross, I. Matthews, Jeffrey F. Cohn, Takeo Kanade, and Simon Baker. Multi-pie. pages 1–8, 2008.
- [40] Rui Huang, Shu Zhang, Tianyu Li, and Ran He. Beyond face rotation: Global and local perception gan for photo-realistic and identity preserving frontal view synthesis. *Proceedings of the IEEE International Conference on*

Computer Vision (ICCV), pages 2458–2467, 2017.

- [41] Dong Chen, Gang Hua, Fang Wen, and Jian Sun. Supervised transformer network for efficient face detection. In *Proceedings of the European conference on computer vision (ECCV)*, 2016.
- [42] Adam Paszke, Sam Gross, Francisco Massa, Adam Lerer, James Bradbury, Gregory Chanan, Trevor Killeen, Zeming Lin, Natalia Gimelshein, Luca Antiga, Alban Desmaison, Andreas Köpf, Edward Yang, Zach DeVito, Martin Raison, Alykhan Tejani, Sasank Chilamkurthy, Benoit Steiner, Lu Fang, Junjie Bai, and Soumith Chintala. Pytorch: An imperative style, high-performance deep learning library. In *NeurIPS*, 2019.
- [43] Diederik P Kingma and Jimmy Ba. Adam: A method for stochastic optimization. In *International Conference on Learning Representations (ICLR)*, page n.pag, 2015.
- [44] Ilya Loshchilov and Frank Hutter. SGDR: Stochastic Gradient Descent with Warm Restarts. In *International Conference on Learning Representations (ICLR)*, page n.pag, 2016.
- [45] Tianye Li, Timo Bolkart, Michael J. Black, Hao Li, and Javier Romero. Learning a model of facial shape and expression from 4D scans. *ACM Transactions on Graphics (TOG)*, 36(6), 2017. URL <https://doi.org/10.1145/3130800.3130813>.
- [46] L. Paul Chew. Constrained delaunay triangulations. *Algorithmica*, 4:97–108, 1989.
- [47] N. Ramanathan and R. Chellappa. Face verification across age progression. *IEEE Transactions on Image Processing (TIP)*, 15(11):3349–3361, 2006. doi: 10.1109/TIP.2006.881993.

VII. APPENDIX

In this part, we provide more visualization results with 3DMM texture (Fig. 15, Fig. 16, Fig. 17).



Fig. 15. DF-MVR Results with 3DMM Texture. The blue dots are the groundtruth of the 2D landmarks, and the red dots represent the projection of the corresponding 3D points which we predict.

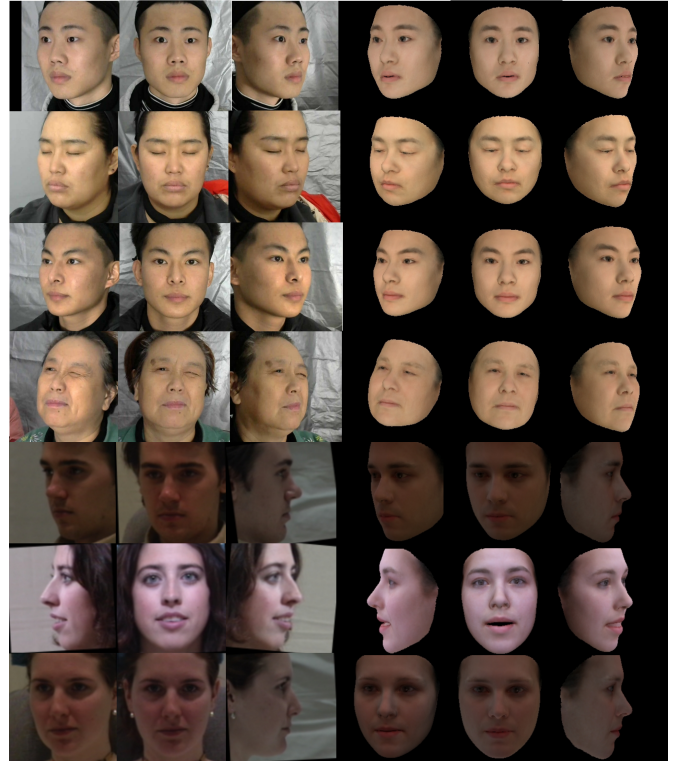


Fig. 16. DF-MVR Results with 3DMM Texture (w/o $L_{l_{3d}}$). We selected samples of different ages, races, angles, and light environments for display. The samples are from the validation set of Pixel-face and Multi-PIE dataset.

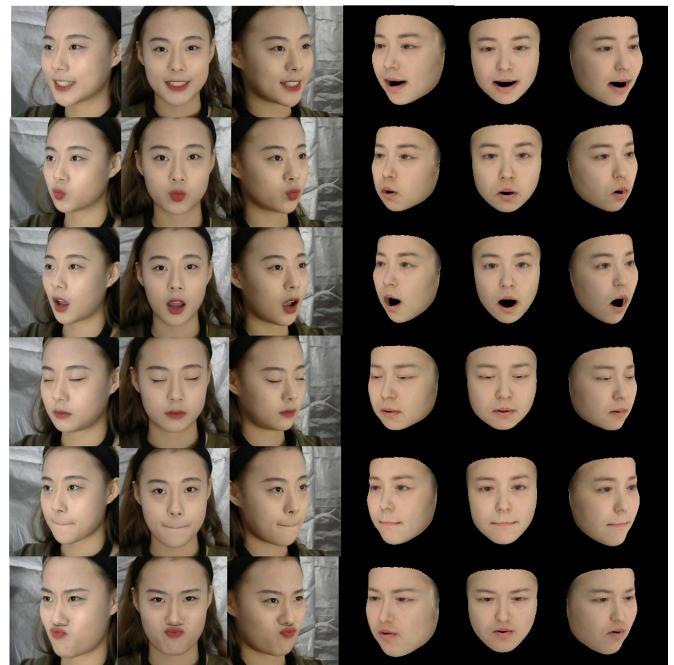


Fig. 17. DF-MVR Results with 3DMM Texture. We provide multiple expression reconstruction results of the same person to show the effectiveness of our model